# OPTIMIZATION DESIGN OF CORE FLOW DISTRIBUTION FOR 45MW SOLID FUEL MOLTEN SALT REACTOR

*Qiaohui Su[1,2,4], Ye Dai[1,2,3*], Fangyuan Zhang[1,2,3], Yang Zou[1,2,3]*

[1]*Shanghai institute of Applied Physics, Chinese Academy of Sciences, Shanghai 201800, China*
[2]*National Key Laboratory of Thorium Energy, Shanghai Institute of Applied Physics, Chinese Academy of Science, Shanghai 201800, China*
[3]*University of Chinese Academy of Sciences, Beijing 101408, China*
[4]*ShanghaiTech University, Shanghai 201210, China*
**daiye@sinap.ac.cn*

**Keywords**: MOLTEN SALT REACTOR-SOLID FUEL (MSR-SF), FLOW DISTRIBUTION, LOWER PLENUM CONFIGURATION, COMPUTATIONAL FLUID DYNAMICS (CFD)

## Abstract

The Molten Salt Reactor-Solid Fuel is a Generation IV advanced nuclear reactor concept where optimal core flow distribution is crucial for efficient nuclear heat removal. The core's hydraulic configuration significantly influences flow distribution characteristics. This study aims to optimize the hydraulic configuration of a 45MW solid fuel molten salt reactor to match flow distribution with power distribution in the core. A one-twelfth scale core model of the 45MW solid fuel molten salt reactor is developed in this investigation. To systematically evaluate the effects of varying downcomer annulus widths, lower plenum heights, and geometries on flow distribution, three-dimensional computational fluid dynamics (CFD) simulations are conducted. The results demonstrate that increasing the width of the descending annulus and the height of the lower chamber can reduce the molten salt velocity in the lower chamber, thereby enhancing flow distribution consistency. Nevertheless, excessive height of the lower chamber can induce vortex formation within it, leading to flow distribution non-uniformity. The standard deviation of matching factor initially decreases from14.2%% to 6.2%, and then increases to 23.5% with increasing lower plenum height. Compared to an elliptical lower plenum, the cylindrical configuration enhances flow distribution uniformity, reducing the standard deviation of matching factor to 6.1%. Additionally, incorporating a flow distribution plate in the lower plenum more effectively suppresses vortex formation. Based on the above analysis, optimal parameters are determined, providing valuable guidance for the engineering optimization of solid-fuel molten salt reactors.

## 1 Introduction

Molten salt reactor-solid fuel (MSR-SF), as a key component of Generation IV nuclear energy systems[1], possesses distinct advantages such as inherent safety, operational reliability, near-atmospheric pressure operation, high-temperature capability, and compact modular design potential [2-4]. Its compact small modular design is suitable for a wide range of applications, including Antarctic research stations, floating nuclear power plants, island development programs, military facilities, and other scenarios[5]. The design of core flow distribution is an essential component of the reactor thermal-hydraulic design and plays a significant role in ensuring the safe operation of the reactor[6]. The 45 MWth MSR-SF reactor features a compact core design with dimensions of 3 m in both diameter and height. When coupled with a high-efficiency Brayton cycle power conversion system, the reactor achieves a net electrical output of 20 MWe. The compact core configuration enables deployment in spatially constrained installations, such as on barges, and functions as a versatile power supply. Furthermore, the system can produce in excess of 50,000 $m^3$/day of potable water through reverse osmosis desalination[7]. The reactor employs a closed-loop circulation channel, with no flow exchange between fuel blocks. As the coolant flows through the downcomer annular into the lower plenum, its direction changes by nearly 90°. This leads to the formation of multiple vortices and small stagnant flow regions within the lower plenum[8,9], resulting in non-uniform flow distribution in the core, which ultimately causes local core temperatures to exceed limits, thereby adversely affecting core material performance and reactor safety. Therefore, conducting research on the core flow distribution characteristics of solid-fueled molten salt reactors is of great significance.

Numerical simulations employing Computational Fluid Dynamics (CFD) have been extensively applied to the analysis of reactor core flow distribution[10]. Yu[11] conducted comparative experimental studies on core inlet flow distribution in CAP1400 reactors employing both flow straighteners and diversion shrouds. Numerical validation using the Realizable k-ε turbulence model demonstrated superior flow uniformity at the core inlet with flow straightener configurations compared to diversion shroud designs. Zhang et al.[12] conducted CFD simulations to

evaluate various flow distribution structures in pressurized water reactors (PWRs). Their results demonstrated that both flow distribution cylinders and semi-ellipsoidal flow distributors significantly improve flow field characteristics in the lower plenum region. Guo et al.[13] developed a detailed computational model of the lower plenum structure and simulated the flow field under optimal flow conditions. The results indicate that while the coolant outlet flow distribution maintains overall uniformity, it exhibits a gradual radial attenuation from the central to peripheral regions. Wang et al.[14,15]performed three-dimensional CFD simulations on three types of flow distributors in the lower plenum of the 1/5-scale four-loop test facility "BORA" namely, a double-layer plate flow distributor, a flow guide baffle, and a spherical flow distributor. The standard k-epsilon turbulence model was employed to investigate and analyze the impact of different internal structures on the flow characteristics within the lower plenum. The results indicated that the core inlet mass flow distribution was more uniform when using the ellipsoidal porous drum and internal structure support. Young min Bae et al.[16] completed the core modeling of the integral SMART (System-integrated Modular Advanced Reactor). Flow distribution analysis at the inlet was conducted using the SST model and the Realizable k-epsilon model. The results indicated that the flow distribution at the core inlet was nearly identical for both turbulence models. The lower core support plate (LCSP) effectively distributes the flow at the SMART core inlet. PODILA K et al.[17] employed an independent CFD approach to simulate the configuration of the Molten Salt Reactor Experiment (MSRE) at Oak Ridge National Laboratory (ORNL). The results highlighted the capability of CFD to predict three-dimensional effects, especially in the lower plenum, within the computational domain. The predicted trends of fuel and coolant temperature increases within the core closely matched the data from ORNL. ROUCH H et al.[18] performed thermal-hydraulic investigations on the core of the Molten Salt Fast Reactor (MSFR). CFD results indicated that the core chamber with curved walls and inlet/outlet legs can achieve a relatively uniform temperature distribution without the need for lower core internals (e.g., perforated plates) to enhance fluid mixing. Wang[19] performed three-dimensional modeling of a one-twelfth core of a 20MWth small modular solid fuel molten salt reactor using STAR CCM+ software, taking into account the effects of interstitial cooling between fuel blocks and mass flow distribution. The study optimized the core temperature distribution and lowered the peak temperatures of the fuel and coolant. The reduction in peak temperatures of the fuel and coolant in the reactor core resulted in a more uniform temperature distribution, preliminarily indicating the feasibility of the current small modular molten salt reactor design.

In summary, although extensive experimental and numerical investigations of core flow distribution have been conducted for PWRs, research specifically targeting MSR-SF remains limited. Moreover, there are currently no mature engineering design solutions available for reference in MSR applications. Therefore, this study employs CFD methodology to perform numerical simulations of core flow distribution in a 45 MWth prismatic molten salt reactor-solid fuel. The study optimizes coolant flow distribution in the reactor core through lower plenum structural modifications and flow distributor implementation, achieving enhanced matching between molten salt channel flow distribution and power distribution. These findings will provide technical references for optimizing the core configuration of solid-fuel molten salt reactors.

## 2 Numerical Method

### *2.1 Geometric model*

The prototype structure of the 45 MWth MSR-SF core and the direction of molten salt flow are illustrated in Fig. 1. The reactor body comprises key components such as the downcomer annulus, core activity zone, radial and axial graphite reflectors, upper and lower plenums, upper and lower metal support plates, and the outer alloy containment vessel. The coolant salt flows downward via the downcomer annulus into the lower plenum. After flow redistribution, it flows upward into the core activity zone, carrying away the heat generated by the TRISO particles in the activity zone, and then exits the core after being collected in the upper plenum. Detailed core structural parameters are provided in Table 1.

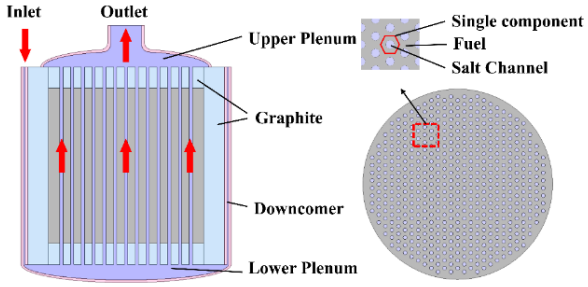


Fig. 1 Schematic illustration of the overall core and single component structure

Table 1. Design parameters

| Parameters | Value |
|---|---|
| Diameter of activity zone(mm) | 3000 |
| Height of activity zone(mm) | 3000 |
| Thickness of radial reflector(mm) | 400 |
| Height of axial reflector(mm) | 800 |
| Number of single components | 445 |
| Diameter of salt channel (mm) | 60 |
| Borderline of single components(mm) | 120 |

Given the complexity and symmetry of the actual core structure, the geometric model is simplified to conserve computational resources. A one-twelfth sector structure is chosen for the calculation, comprising 52 single components. To study the flow distribution characteristics of molten salt within the reactor, sensitivity analyses are performed on the width of the downcomer annulus ($D$), the height of the lower plenum ($H$), and the geometry of the lower plenum. The specific structural parameters are provided in Table 2.

Table 2. Range of parameters

| Parameters | Value |
|---|---|
| Width of the downcomer annulus *D*(mm) | 30-50 |
| Height of the lower plenum *H*(mm) | 100-400 |
| Geometry of the lower plenum | Ellipsoid, Cylinder |

*2.2 Grid generation and model validation*

To ensure computational accuracy, this study performs mesh-independence and turbulence model comparison analyses for the elliptical lower plenum structure with *D*=30 mm and *H*=300 mm. Meshing is conducted using Fluent Meshing. All computational domains utilize unstructured grids, with mesh refinement at the fluid-solid interface. Four different meshing approaches are employed, with the mesh count varying from 3 million to 12 million. The minimum orthogonal mesh quality is 0.2, and the skewness is maintained below 0.8, satisfying the precision requirements for CFD calculations. The results of calculations with different meshes are illustrated in Fig. 2. The results indicate that when the mesh size exceeds 8.6 million (mesh3), the flow distribution in the radial direction of the core channels remains essentially unchanged. It can be concluded that the mesh density no longer impacts the calculation results. All subsequent calculations are conducted using the third meshing approach.

In this study, the average Reynolds number in the core activity zone is approximately 6900, corresponding to turbulent flow conditions. Fig. 3 presents a comparison of the calculation results obtained using different turbulence models (Standard k-ε model, RNG k-ε model, Realizable k-ε model). The results indicate that the radial variation trends of flow in different channels are essentially consistent across various turbulence models. Given that this study focuses solely on qualitative analysis of the core mass flow distribution[20], and taking into account the stability of model convergence and the constraints on computational resources, the robust Standard k-epsilon model is chosen for subsequent numerical studies.

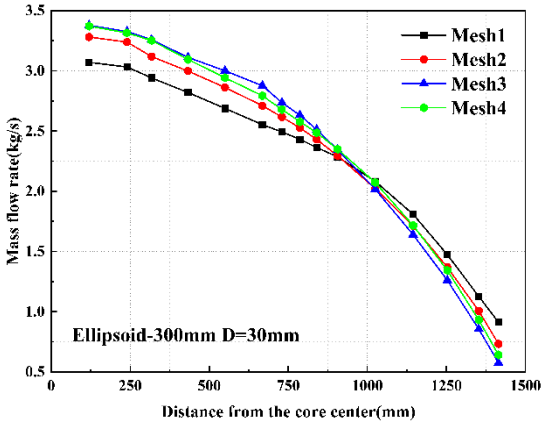


Fig. 2 Grid independence analysis

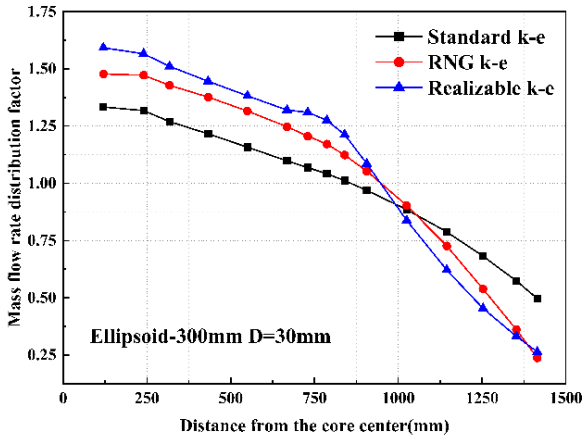


Fig. 3 Comparison of different turbulence models

*2.3 Model Setup*

The molten salt inlet is specified as a mass flow inlet with a flow rate of 85.73 kg/s and an inlet temperature of 600°C. The outlet is specified as a constant pressure outlet. The interfaces between fuel, molten salt, graphite, and alloy are defined with conjugate heat transfer and no-slip boundary conditions. All other surfaces are defined as adiabatic boundaries. A pressure-based implicit double-precision solver is employed, and the SIMPLE algorithm is used to compute the velocity-pressure coupling. The calculation is deemed converged when the residuals of the governing equations fall below $10^{-6}$ and the monitored inlet pressure and outlet temperature remain unchanged.

The radial and axial power distributions of the core are calculated using the Monte Carlo N-Particle Transport Code (version 5, MCNP5) and are directly applied to the core graphite fuel region. The core radial power factor decreases as the radial distance increases, varying between 0.75 and 1.16. The axial power distribution factor exhibits a parabolic trend, initially increasing and then decreasing with height, varying between 0.32 and 1.43. These distributions are illustrated in Fig. 4 and 5.

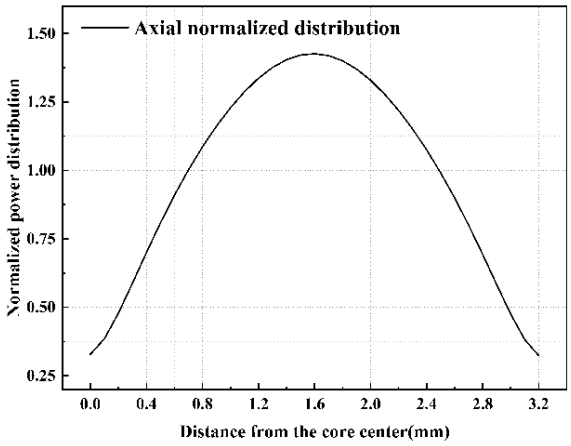


Fig. 4 Normalized axial power distribution

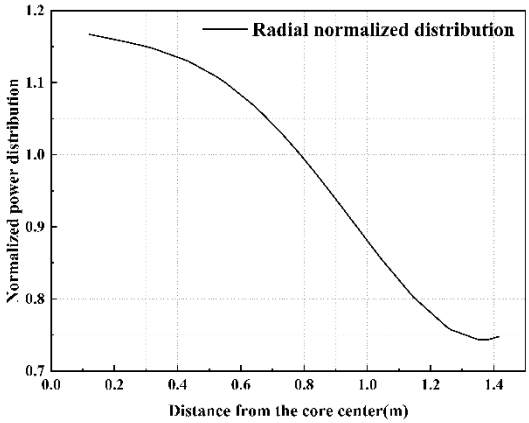


Fig. 5 Normalized radial power distribution

The MSR-SF is designed with a thermal power of 45MW. Graphite is employed as the moderator, and FNaBe salt serves as the coolant. The specific physical properties are provided in Table 3. TRISO particles are randomly dispersed within the components. Detailed modeling of TRISO particles is challenging in practical calculations. Thus, the components are subjected to volumetric homogenization, and the equivalent thermal conductivity is calculated using the Maxwell - Eucken model[21] , as given in Equation 1.

$$k_f = k_m \frac{k_p+2k_m+2V_p(k_p-k_m)}{k_p+2k_m-V_p(k_p-k_m)} \quad (1)$$

In the equation, $k_f$, $k_p$, and $k_m$ denote the thermal conductivities of the components, fuel particles, and matrix, respectively. $V_p$ indicates the volume fraction of fuel particles within the components.

Table 3. Thermal and physical properties of molten salts and solid materials

| Materials | Density/ kg·m$^{-3}$ | Specific heat capacity/J·kg$^{-1}$·°C$^{-1}$ | Thermal conductivity/ W·m$^{-1}$·°C$^{-1}$ | Dynamic viscosity/ Pa·s |
|---|---|---|---|---|
| FNaBe | 2270-0.0 0037T | 2177 | 0.87 | 0.00035exp (5165/T) |
| Graphite | 1779 | 1780 | 59.09 | — |
| Alloy | 8860 | 565 | 20.3 | — |
| Fuel | 1819.5 | 2102.5 | 55.5 | — |

*2.4 Parameter definition*

In accordance with the design objectives for core flow distribution, this study establishes two key evaluation metrics for optimizing flow distribution: one is the correspondence between the mass flow distribution and the power, and the other is the pressure drop associated with core flow. The mass flow distribution and power matching factor in molten salt channels：

$$\lambda_{Di} = \lambda_i - q_i \quad (2)$$

In the equation, $q_i$ denotes the normalized power factor at various radial positions, while $\lambda_i$ signifies the mass flow distribution factor for the molten salt channels at these radial positions.

To more effectively evaluate the overall matching performance of each component, the standard deviation of matching factor, $\sigma$, is introduced to quantify the variability of the mass flow distribution and power matching across different radial positions, as expressed in Equation 3. A lower σ value signifies a superior alignment between flow and power distributions.

$$\sigma = \sqrt{\frac{\sum_i {\lambda_{Di}}^2}{n-1}} \quad (3)$$

## 3 Results and Discussion

*3.1 Influence of downcomer annulus width on Flow Distribution*

The downcomer annulus, which is formed by the annular gap between the reactor pressure vessel (RPV) and core barrel, serves to guide and stabilize the primary coolant (molten salt) flow from the primary circuit piping into the core region. This critical flow path suppresses turbulence generation and ensures hydrodynamic smooth transition at the lower plenum inlet. Furthermore, the relatively cooler molten salt within the downcomer facilitates passive heat removal from adjacent core structures through thermal conduction in the graphite reflector. The downcomer annulus has two critical geometric parameters: height and width. With the annulus height substantially exceeding its hydraulic diameter ($L/D_h$>100), the flow maintains fully developed characteristics. The annulus width directly determines the coolant entry velocity into the lower plenum. Excessive velocity may induce jet impingement phenomena, which not only disturbs core inlet flow distribution but also pose risks material erosion through hydrodynamic impact forces.

This study conducts comparative analyses for three downcomer annulus widths ($D$=30 mm, 40 mm, and 50 mm), with computational results presented in Fig. 6. For all width configurations, the flow distribution across core channels exhibits a consistent radial attenuation pattern, decreasing progressively from central to peripheral regions. Increasing the downcomer annulus width demonstrates limited influence on inter-channel flow distribution. When the width expands from 30 mm to 50 mm, the maximum mass flow factor decreases marginally from 1.33 to 1.29, while the standard deviation of matching factor improves from 10.77% to 9.05%. To further elucidate the molten salt flow characteristics, Fig. 7 presents streamline diagram of the lower plenum flow field for different annulus widths. As the downcomer width increases, the expanded flow area reduces coolant velocity, thereby attenuating jet impingement effects upon lower plenum entry. This velocity reduction promotes enhanced flow diversion toward peripheral channels, improving overall flow distribution uniformity. Furthermore, the decreased flow velocity reduces system pressure losses, with experimental data showing a 40% reduction in pressure drop when the annulus width expands from 30 mm to 50 mm.

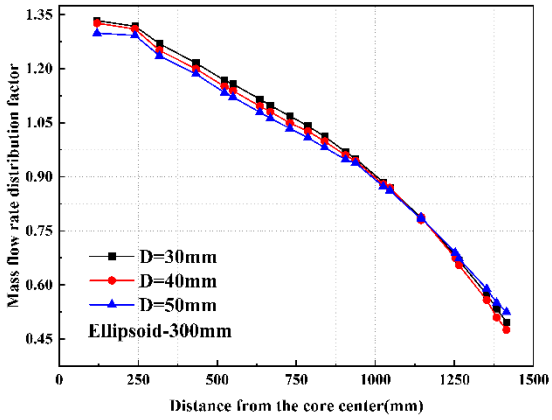


Fig. 6 Flow factors for different downcomer annulus widths

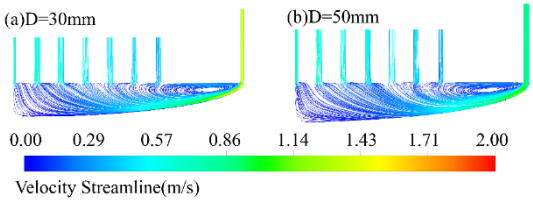


Fig. 7 Streamline diagram for various downcomer annulus widths

### *3.2 Influence of lower plenum height on flow distribution*

The lower plenum serves as a key structural interface between the downcomer annulus and the lower reflector flow channels. It primarily facilitates the transitional flow distribution of molten salt and critically governs the flow distribution within the reactor core. A systematic sensitivity analysis is performed for lower plenum heights ($H$) of 100mm, 200mm, 300mm, and 400mm. The numerical results are presented in Fig. 8. The optimal flow distribution uniformity across core channels is achieved at $H$=200mm. Deviation from this optimal height (either increase or decrease) deteriorates the flow distribution characteristics. Increasing $H$ from 100mm to 200mm reduces the standard deviation of matching factor from 14.1% to 6.2%. However, further elevation to 400mm increases this parameter from 6.2% to 23.4%. To elucidate the impact of lower plenum height on flow distribution behavior, Fig. 9 presents the streamline diagram corresponding to varying plenum heights. At an inadequate plenum height ($H$=100mm), owing to the wall confinement effect in the elliptical plenum, the bulk molten salt flow is preferentially directed to the central channels, creating flow deficiency in peripheral regions and thereby compromising flow distribution uniformity. Furthermore, the increased flow velocity induces significant additional pressure losses. Increased plenum heights decrease the molten salt flow velocity, promoting enhanced flow distribution to peripheral regions and thereby optimizing flow distribution uniformity. However, at excessive plenum heights ($H$=300mm, 400mm), significant vortex formation occurs along the plenum periphery. These vortices disrupt the flow distribution in peripheral channels while concurrently increasing the plenum pressure drop, thereby imposing additional operational burdens on the primary coolant pump.

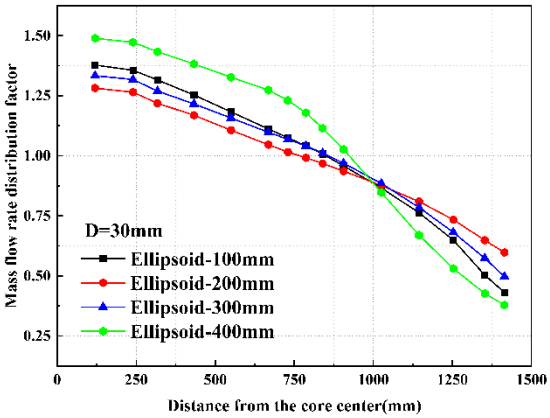


Fig. 8 Flow factors for different lower plenum heights

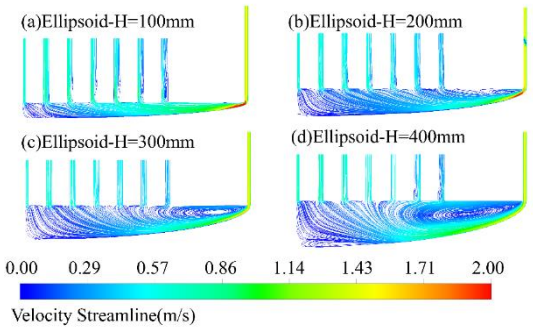


Fig. 9 Streamline diagram for different lower plenum heights

### *3.3 Influence of lower plenum geometry on flow distribution*

The curved contour of conventional elliptical lower plenums induces preferential flow focusing toward central channels, significantly compromising flow distribution homogeneity. To mitigate this effect, this study proposes a cylindrical lower plenum design incorporating an optimized flat base geometry. A comprehensive parametric study is conducted to assess flow distribution characteristics across varying plenum heights (100-400mm) and geometric configurations, with comparative results systematically presented in Fig. 10. The results demonstrate that the cylindrical configuration with $H$=100mm plenum height achieves optimal flow distribution characteristics, exhibiting the standard deviation of matching factor of 6.05%. Conversely, the worst performance occurs with cylindrical $H$=300mm configuration, showing 13.8% standard deviation. Notably, the $H$=300mm case produces significantly elevated flow distribution in channels at 900mm radial distance from core center. Fig. 11 presents the streamline diagram within cylindrical lower plenums of varying heights. The flow visualization reveals that upon entering from the downcomer annulus, in contrast to elliptical configurations, the molten salt flow exhibits different characteristics. Owing to the flat base geometry of cylindrical plenums, the jet flow characteristics are significantly attenuated and the flow velocity magnitude is reduced, consequently diminishing the flow rate disparity between central and peripheral regions. At increased cylindrical

plenum heights ($H$=300mm), more pronounced vortex structures develop within the plenum. This vortex-induced flow redirects molten salt toward intermediate regions between central and peripheral zones, consequently compromising flow distribution homogeneity. Furthermore, in contrast to elliptical plenum configurations, the cylindrical geometry attenuates molten salt jetting behavior, and this velocity reduction yields a 10-41% decrease in pressure losses.

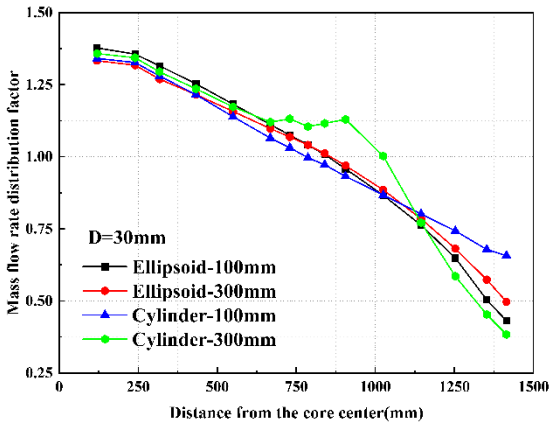


Fig. 10 Flow factors for different lower plenum geometry

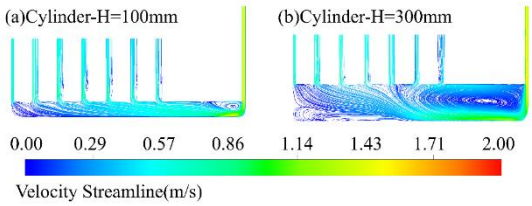


Fig. 11 Streamline diagram for different lower plenum geometry

*3.4 Influence of flow distribution plate on flow distribution*

To address the localized vortex formation observed in cylindrical plenums (Section 3.3), a flow distribution baffle system is implemented within the plenum to effectively mitigate vortex generation and development. The baffle configuration is illustrated in Fig. 12. The primary structure consists of vertical flat plates, with a 10mm chamfer incorporated at the downcomer interface to gradually transition the molten salt flow. Strategically spaced orifices are designed across the core inlet region - the central orifices (60mm diameter) are positioned along the axial region, while larger peripheral orifices (100mm diameter) are arranged radially outward. The flow distribution assembly is mounted on the reactor core's lower support plate, with its centerline aligned with the lower plenum's mid-plane. To facilitate computational modeling, the structural connections between the support plate and distribution assembly are simplified in the numerical model. The computational results are illustrated in Fig. 13 and 14. The flow distribution plate has minimal impact on the flow distribution characteristics, and it incurs additional pressure loss. However, the local vortices originally present near the exit section of the annulus are essentially eliminated due to the effect of the distribution plate. Therefore, the flow distribution plate can be regarded as an effective measure for suppressing vortices in the lower plenum.

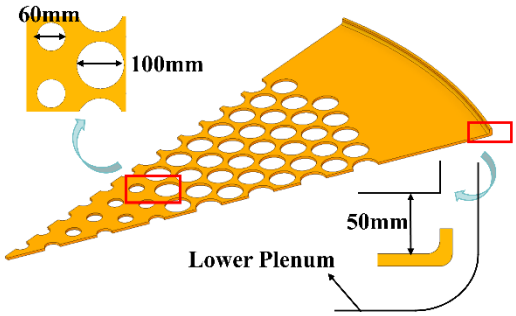


Fig. 12 Schematic of flow distribution plate structure

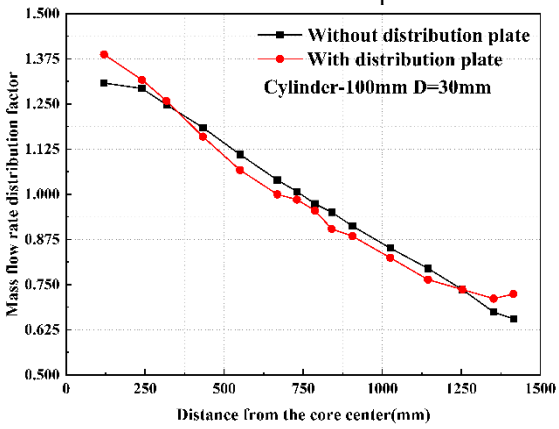


Fig. 13 Flow factors for flow distribution plate

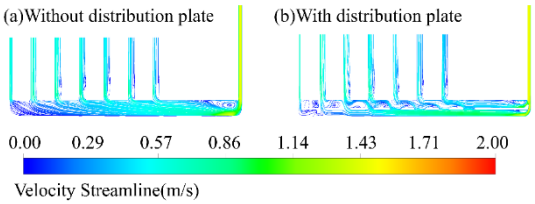


Fig. 14 Streamline diagram of the lower plenum with and without a flow distribution plate

Table 4 presents a comprehensive summary of the flow distribution characteristics for 11 different configurations of the lower plenum and downcomer annulus. The results demonstrate that the optimal flow-power matching characteristics are achieved with a cylindrical lower plenum having a height $H$=100 mm and a downcomer annulus width $D$=30 mm. For this configuration, the standard deviation $\sigma$ is 6.1%, and the pressure drop is 8417 Pa.

Table 4. Flow distribution characteristics in the core with different structural parameters

| Case | $D$(mm) | $H$(mm) | Geometry | $\sigma$ | Pressure (kPa) |
|---|---|---|---|---|---|
| 1 | 30 | 300 | Ellipsoid | 10.8% | 9.0 |
| 2 | 40 | 300 | Ellipsoid | 10.9% | 6.6 |
| 3 | 50 | 300 | Ellipsoid | 9.1% | 5.5 |
| 4 | 30 | 100 | Ellipsoid | 14.2% | 14.5 |

| | | | | | |
|---|---|---|---|---|---|
| 5 | 30 | 200 | Ellipsoid | 6.2% | 9.7 |
| 6 | 30 | 400 | Ellipsoid | 23.5% | 9.2 |
| 7 | 30 | 100 | Cylinder | 6.1% | 8.4 |
| 8 | 30 | 200 | Cylinder | 14.9% | 7.4 |
| 9 | 30 | 300 | Cylinder | 17.4% | 8.2 |
| 10 | 30 | 400 | Cylinder | 13.8% | 8.3 |
| 11 | 30 | 100 | Cylinder (With distribution plate) | 7.6% | 8.7 |

## 4 Conclusion

This study employs the CFD numerical analysis software FLUENT to optimize the inlet structure of 45 MWth MSR-SF. A comprehensive investigation of the flow distribution characteristics has been conducted. The primary conclusions drawn are as follows:

(1) The width of the downcomer annulus has a relatively minor impact on the flow distribution characteristics, but it can reduce the total pressure loss within the downcomer annulus and the lower plenum substantially. When the downcomer annulus width $D$ is increased from 30 mm to 50 mm, the standard deviation of matching factor decreases from 10.77% to 9.1%, and the pressure drop is reduced by 40%.

(2) The uniformity of core flow distribution initially increases and then decreases as the height of the lower plenum increases. When $H$ is 200 mm, the flow-power matching is the best, with the standard deviation of matching factor being 6.2%.

(3) Compared with the ellipsoidal lower plenum structure, the cylindrical lower plenum structure demonstrates superior flow distribution uniformity. Additionally, the decrease in flow velocity within the lower plenum further reduces pressure loss. However, an excessively tall cylindrical lower plenum can instead deteriorate the core flow distribution. The optimal configuration is a cylindrical lower plenum with a height of 100 mm, for which the standard deviation of matching factor is 6.1%.

(4) The installation of a flow distribution plate in the lower plenum effectively mitigates vortices in the vicinity of the downcomer annulus. However, this approach compromises the matching between flow and power to some extent.

The final optimization scheme features a cylindrical lower plenum, 100 mm in height, and a downcomer annulus width of 30 mm, with a pressure drop of 8.4 kPa and a standard deviation $\sigma$ of 6.1%. These conclusions can provide valuable guidance for optimizing the core flow distribution in the Molten Salt Reactor-Solid Fuel.

## 5 Acknowledgements

This research was funded by Fundamental Research Program of Industrial Foundation (SINAP-CYJJ-202503).

## 6 References

[1] Holcomb D, Ilas D, Qualls A, et al.:'Current Status of the Advanced High Temperature Reactor'. 2012.

[2] Holcomb D, Ilas D, Varma V, et al.:'Core and Refueling Design Studies for the Advanced High Temperature Reactor'. 2011.

[3] Ingersoll D, Forsberg C, Ott L, et al.:'Status of Preconceptual Design of the Advanced High-Temperature Reactor (AHTR)'. 2004.

[4] Zhou C X, Min D Z, Jie X H.:'Thorium molten salt reactor nuclear energy system'. Physics, 2016, 45(09), pp.578-90.

[5] Dai Z.':17 - Thorium molten salt reactor nuclear energy system (TMSR)'. Molten Salt Reactors and Thorium Energy, 2017, pp.531-40.

[6] Kania M J, Nabielek H, Verfondern K, et al.:'Testing of HTR UO2 TRISO fuels in AVR and in material test reactors'. Journal of Nuclear Materials, 2013, 441(1), pp.545-62.

[7] Haider S.:'Theoretical calculation simulation studies of ABV nuclear reactor coupled with desalination system'. International Journal of Energy Research, 2015, 39.

[8] Shuming Z, Huaqi L, Minfuo, Z, et al.:'Numerical analysis of flow distribution at the reatorcore inlet of Qinshan phase-II reactor'. Chinese Journal of Nuclear Science and Engineering, 2010, 30(04), pp.299-307.

[9] Böttcher M, Krüßmann R.'Primary loop study of a VVER-1000 reactor with special focus on coolant mixing'. Nuclear Engineering and Design, 2010, 240(9), pp.2244-53.

[10] Luzzi L, Cammi A, Di Marcello V, et al.:'An approach for the modelling and the analysis of the MSR thermo-hydrodynamic behaviour'. Chemical Engineering Science, 2010, 65(16), pp.4873-83.

[11] Fan Y.'Experiment Study on CAP1400 Core Inlet Flow Distribution'.PhD thesis,Shanghai Jiao Tong University, 2017.

[12] Zhang H, Liu H, Fang C s, et al.:'Optimized design of reactor lower chamber structure'. Nuclear Power Engineering, 2014, 35(03), pp.59-63.

[13] Guo C, Wei C, Tian X, et al.:'Numerical Simulation Analysis of Flow Characteristics in Lower Plenum of Pressure Water Reactor'. Nuclear Science and Engineering, 2018, 38(03), pp.353-8.

[14] Wang M, Wang L, Wang X, et al.:'CFD simulation on the flow characteristics in the PWR lower plenum with different internal structures'. Nuclear Engineering and Design, 2020, 364, pp.110705.

[15] Xu T, Min J, Bellet S, et al.:'Design Investigation on Flow Diffuser With Code_Saturne: CFD Simulation Analysis'; the 2017 25th International Conference on Nuclear Engineering,Shanghai, China,2017.

[16] Bae Y, Kim Y I, Park C T.:'CFD analysis of flow distribution at the core inlet of SMART'. Nuclear Engineering and Design, 2013, 258, pp.19-25.

[17] Podila K, Qi C, and Rao Y.:'CFD Simulations of Molten Salt Reactor Experiment Core'. Nuclear Science and Engineering, 2019, 193(12), pp.1379-93.

[18] Rouch H, Geoffroy O, Rubiolo P, et al.:'Preliminary thermal–hydraulic core design of the Molten Salt Fast Reactor (MSFR)'. Annals of Nuclear Energy, 2014, 64, pp.449-56.
[19] Wang C, Sun K, Zhang D, et al.:'Thermal-hydraulic design and analysis of a small modular molten salt reactor (MSR) with solid fuel'. International Journal of Energy Research, 2018, 42(3), pp.1098-114.
[20] Ping C J, Ming Y L, Chen L F.:'CFD simulation of a four-loop PWR at asymmetric operation conditions'. Nuclear Engineering and Design, 2016, 300, pp.591-600.
[21] A Treatise on Electricity and Magnetism'. Nature, 1873, 7(182), pp.478-80.